BOLLETTINO DI GEOFISICA TEORICA ED APPLICATA VOL. XXXVII, N. 148 - DECEMBER 1995

E. CARDARELLI

# 3D TOMOGRAPHY OF SOME PILLARS OF THE COLISEUM

**Abstract.** A few years ago a 2D tomographic survey was carried out (Bernabini et al., 1990) on some pillars of the Coliseum. To cover a greater portion of the pillars and with the aim of clearly defining the velocity field and thus identifying any evidence of vertical variations, it was decided to enlarge the research by carrying out a 3D tomographic survey on the same pillars. The LSQR was the resolution algorithm utilized and the results obtained will be discussed and analysed.

## INTRODUCTION

In the field of applied geophysics, tomographic techniques are not only a valid tool for determining elastic properties on sites of large engineering plants, but they are an important aid in evaluation of the state of conservation of monuments.

With this aim, a bidimensional tomographic survey was carried out a few years ago (Bernabini et al., 1990) on some pillars of the Coliseum by placing horizontally at a certain height on the pillars a number of electro-acoustical sensors and source points.

The survey led to some interesting conclusions. In fact it was ascertained that the joints between the travertine blocks that formed the pillars had no influence on the recordings. Thus the blocks must be well joined. Furthermore, the travertine blocks presented differences from one pillar to another and within a single pillar that could be attributed to differences in the raw material at the time of construction and to the decay of the material caused by man, weathering and strains from static and dynamic stresses due to earthquakes in 2000 years of history. To enlarge the research to cover a greater portion of the pillars and to place in greater evidence the vertical velocity distribution not otherwise detectable, a 3D survey was carried out on the same pillars.

This survey consisted in positioning a series of sensors and source points around the pillars at different levels so that it was possible to obtain both horizontal and dip paths.

## FIELD SURVEY

The survey was carried out on 4 pillars already investigated by 2D tomography (Bernabini et al., 1990). The pillars examined are shown in the planimetry in Fig. 1 and are on the left side of the vaults numbered 53, 49, 45, 43.

The pillars consist of travertine blocks (hewn stone) of variable dimensions placed horizontally,



Manuscript received April 15, 1994; accepted September 25, 1994.

Dip. ITS, Area di Geofisica, Università "La Sapienza", Roma, Italy.

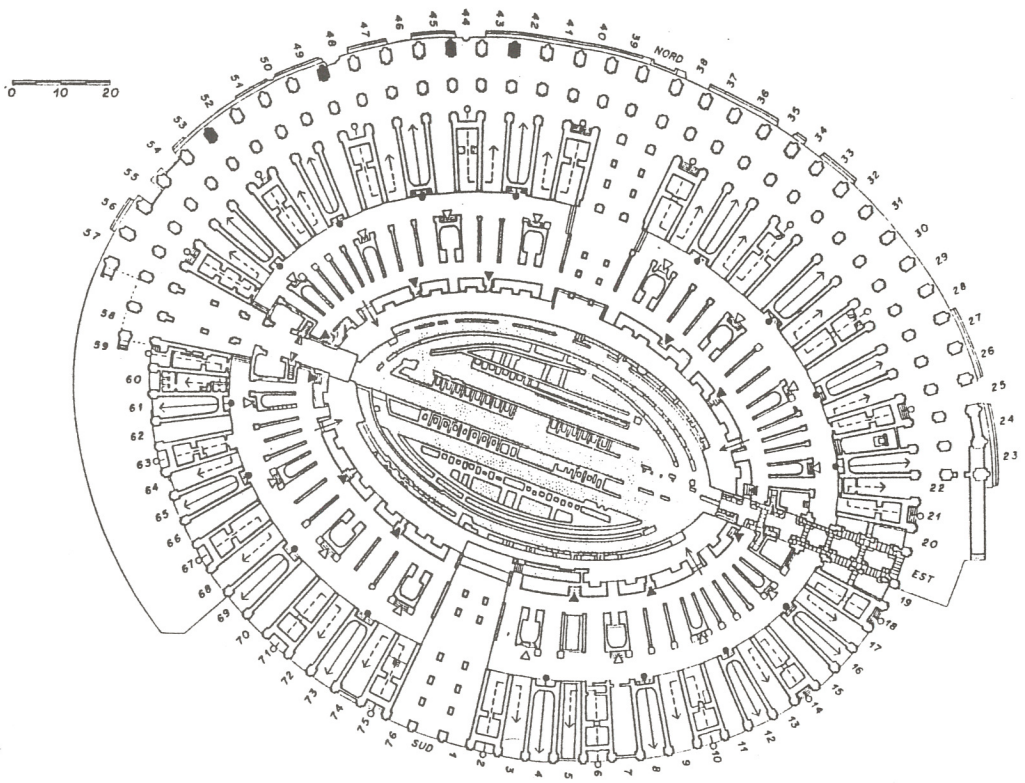


Fig. 1 — Coliseum planimetry.

and with thickness varying from a minimum of 80 cms. to a maximum of 120 cms. To carry out the survey we made use of 23 piezoelectric sensors with cut-off frequency of 4khz placed on three horizontal levels, one above the other, at a distance of approximately 1 m. The sensors covered three sides of the pillar at a distance of 90 cm. between them; the elastic wave source points were placed on four sides of the pillar corresponding to the three levels where the sensors were placed so as to obtain both horizontal and dip paths. The examined volume of each pillar was $3.22 \times 2.30 \times 2.1$ cubic metres. The 24th channel was connected to a piezoelectric sensor in the hammer utilized as a source and functioned as time-break.

The recording instrument utilized was an Abem 24 channel Terraloc with a record length of 24 ms and a 24 $\mu$s resolution. Thirtythree shots were made for each pillar for a total of about 800 raypaths.

Before processing the data, they were subjected to various controls. In particular, paths whose rectilinear seismic rays extended partly beyond the pillars, or those times whose values were outside the predictible range, were eliminated. The rejected times (outliers) were successively controlled and corrected if possible.

After such pre-processing an average of 600 useful projections were left for each pillar.

As a preliminary analysis of the velocity for each single pillar, an average velocity of all paths was considered, as shown here in the following, (Pil. 43 Vm=2257 m/s, Pil. 45 Vm=2200 m/s, Pil. 49 Vm=2044 m/s, Pil. 53 Vm=2200 m/s), and the histograms of the velocities of the same paths (Fig. 2a, b, c and d) were also analysed.

It can be seen that while the average velocities are approximately the same, excluding Pil. 49, the distribution of the velocity values differs from one to another. In fact while pillar 43 presents a bell type distribution in which the maximum number of samples concentrates around 2300 m/s, pillar 45 presents a fairly even distribution in all the considered velocity intervals.

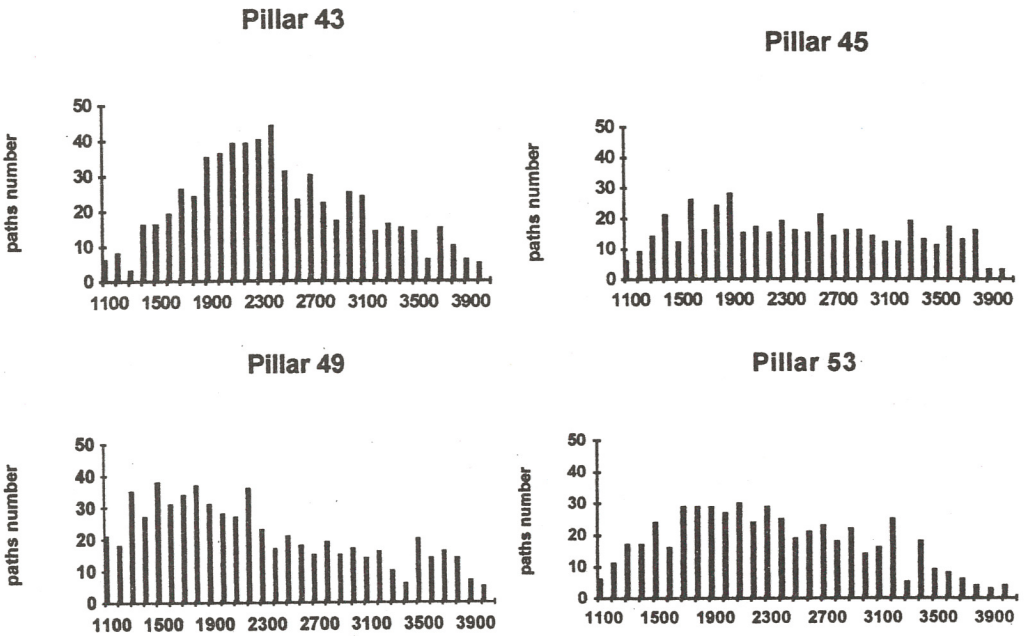


Fig. 2 — Histograms of the velocity distribution for each single path at intervals of 100 m/s.

Pillar 49 has the greater part of its velocity values concentrated at the bottom of the interval considered (1800-2000 m/s), and pillar 53 has a distribution similar to that of pillar 43 with a maximum concentration of around 2300 m/s, although less enhanced.

## METHOD OF ELABORATION

In the tomographic technique used in this study, it was assumed that raypaths were straight and that every cell had a constant P-wave velocity. It is known that the problem is to search for a solution to a linear system of the type

$$\gamma = G^{-1}\, T\,, \tag{1}$$

where $G^{-1}=(A^T\ A)^{-1}\ A^T$ is a square matrix derived from matrix A, whose elements $a_{ij}$ represent the portion of the i-th ray passing through the j-th cell; $\gamma_j$ is the inverse velocity (slowness) of the j-th. cell, and $T_i$ is the arrival time of the complete i-th. ray.

The generalized inverse matrix $G^{-1}$ is a sparse matrix whose elements are nearly all zero. Solving the system of linear equations given by eqn. (1) with the use of a small or medium size calculator can create problems due to the limited amount of memory, and would be quite impossible in the case of a large number of cells. To overcome this problem, great use is now made of iterative systems.

In tomography, different types of algorithms are utilized to resolve linear systems of the above mentioned type. The most commonly used methods are SIRT (Ivansonn, 1983), Conjugate Gradient "CG", and a variation of this last method proposed by Paige and Saunders in 1982, the "LSQR" (Least Squares). Such a method, similar to the inversion methods based on "SVD" (Single Value Decomposition), was discussed by Nolet e Spackman 1988, and Nolet (1987) provided a version of the algorithm in Ratfor.

After a close examination of each single algorithm, the LSQR method was chosen, because it is superior to a SIRT type, both in its suppression of the propagation of rate errors, and

**Table 1 — Cell number and dimensions for each pillar.**

| | Cell dimensions | | | Cell numbers | | | |
|---|---|---|---|---|---|---|---|
| | X m | Y m | Z m | nx | ny | nz | nc |
| Pil 53 | 0.38 | 0.41 | 0.60 | 6 | 8 | 3 | 144 |
| Pil 49 | 0.37 | 0.38 | 0.82 | 6 | 9 | 3 | 162 |
| Pil 45 | 0.37 | 0.40 | 0.86 | 6 | 8 | 3 | 144 |
| Pil 43 | 0.40 | 0.42 | 0.74 | 6 | 8 | 3 | 144 |

in the rate convergence to the true solution (Nolet 1987). This method also provides better results for ill-conditioned systems (Van Der Sluis and Van Der Vost, 1987).

In order to condition the result so as to arrive at an acceptable physical solution, two constraint coefficients were introduced. One was used to minimize the differences in the slowness of each single cell and the average velocity. The second coefficient was used to minimize the slowness between contiguous cells.

In order to obtain a more correct representation of the velocity distribution on the pillar, particular attention was made to the subdivision of the pillar into cells. The pillars were divided in such a way that the cells fell within each single block, and hence their dimensions varied slightly from pillar to pillar. Table 1 shows the dimensions, in metres, of cells (Xm., Ym., Zm.), the number of cells into which the pillars are subdivided in the three orthogonal directions (nx, ny, nz), and the number of resulting cells for each single pillar (nc.). Furthermore, since the blocks within each pillar are not of the same thickness, the value of z represents its average.

## RESULTS OBTAINED

As was already mentioned in the introductory notes, the principle aim of this project is to compare the results obtained by applying 3D and 2D tomographic techniques to the same pillar. Such comparisons can, for example, highlight the presence of any fractural trends or intrinsic anisotropies of the material, because in 2D tomography the results obtained are relative to the horizontal paths, whereas in 3D the results are relative to both horizontal and dip paths. In fact, taking into consideration the whole ray distribution, one 3D tomography can be obtained for each pillar, whereas three 2D tomographies were obtained using only those paths which fell on each of the 3 levels where sensors and shot points were placed. The same subdivision into cells was obviously maintained in both cases.

A comparison between the 2D and 3D interpretations on each considered plane was carried out not only by comparing the total average velocity values but also by comparing the velocity values of the respective cells obtained from the two processings.

To provide a numeric values for such a comparison, a correlation coefficient was calculated for each plane from the following formula:

$$\sigma = \frac{\sum_i (V_{iT} - V_{Tm}) \times (V_{iB} - V_{Bm})}{N \times \sigma_1 \times \sigma_2} \quad , \tag{2}$$

where $V_{iT}$ and $V_{mT}$ are respectively the velocity of the i-th cell, and the average velocity in 3D tomography; $V_{iB}$ and $V_{mB}$ are the corresponding values for the 2D tomography; N is the number of cells considered; and $\sigma_1$ and $\sigma_2$ are the mean square roots of $V_{iT}$ and $V_{iB}$ respectively.

A description and analysis of the results obtained for each pillar is now given.

## PILLAR 43

A visual examination of pillar 43 does not show any particular weathering or fractures.

**Table 2 — Pillar 43; 3D and 2D mean velocity and correlation coefficient values for each plane.**

| | | | |
|---|---|---|---|
| Top plane | $V_{mT}$=2272 m/s | $V_{mB}$=2300 m/s | $\sigma$=0.006 |
| Middle plane | $V_{mT}$=2370 m/s | $V_{mB}$=2700 m/s | $\sigma$=0.253 |
| Bottom plane | $V_{mT}$=2308 m/s | $V_{mB}$=2380 m/s | $\sigma$=0.583 |

The whole structure appears to be intact with the exception of a few zones on the left side of the pillar which suggests that the travertine was subjected to some chemical alteration. Figure 3a gives the 3D tomography and shows that this weathering appears to have spread to the inside of the pillar, where a low velocity (1600-1800 m/s) zone extending from the exterior to the interior can be seen on each of the three planes.

Fig. 3b represents the 2D velocity field contour. Here, the low velocity zone is less evident, which could be attributed to a light anisothropic fracture of the travertine. Table 2 shows the average velocity values of each single plane and also the values of the correlation coefficients. Note how very low these values are.

$V_{mT}$ e $V_{mB}$ are the average velocity values of cells resulting from the 3D and 2D tomography respectively, and $\sigma$ is the correlation coefficient value.

## PILLAR 45

Pillar 45 presents a highlighted zone of low velocity on the right side (Fig. 4a). This zone is restricted to the more superficial area and affects all three planes. The average velocity value (2350 m/s) obtained from the tomographic survey is similar to that of pillar 53 and is one of the highest. Fig. 4b shows the results from the 2D tomography where the low velocity zone has even lower velocity values.

The correlation between the results of the two surveys is higher than that for pillar 43. The similar average velocity values obtained from the two tomographies appears to exclude the presence of anisothropy.

$V_{mT}$ e $V_{mB}$ are the average velocity values of cells from the 3D and 2D tomography respectively, and $\sigma$ is the correlation coefficient value.

## PILLAR 49

By observing the results for pillar 49 (Fig. 5) it can be seen that this is the most damaged pillar. Large low velocity zones are present, extending from within the pillar and covering 2/3 of the pillar down to its lowest plane. The front part of the pillar is an exception where the velocities are relatively high (3400-3800 m/s). This difference in values with respect to the rest of the pillar is explained by the fact that part of the pillar was restored in the last century by partial substitution of a block.

In Fig. 5b, representing the 2D tomography, the area of low velocity on the lower plane appears to increase in size. On the contrary, the behaviour and velocity values of the higher planes remain very similar to that of the 3D tomography. Even in this case, the results confirm what appears on the surface of the pillar; in fact in the lower velocity zone, there is a set of sub-vertical fractures on the middle and lower side of the surface of the pillar. The lower values for the velocity show that these fractures extends into the pillar.

**Table 3 — Pillar 45; 3D and 2D mean velocity and correlation coefficient valves for each plane.**

| | | | |
|---|---|---|---|
| Top plane | $V_{mT}$=2277 m/s | $V_{mB}$=2201 m/s | $\sigma$=0.557 |
| Middle plane | $V_{mT}$=2264 m/s | $V_{mB}$=2241 m/s | $\sigma$=0.601 |
| Bottom plane | $V_{mT}$=2436 m/s | $V_{mB}$=2490 m/s | $\sigma$=0.603 |

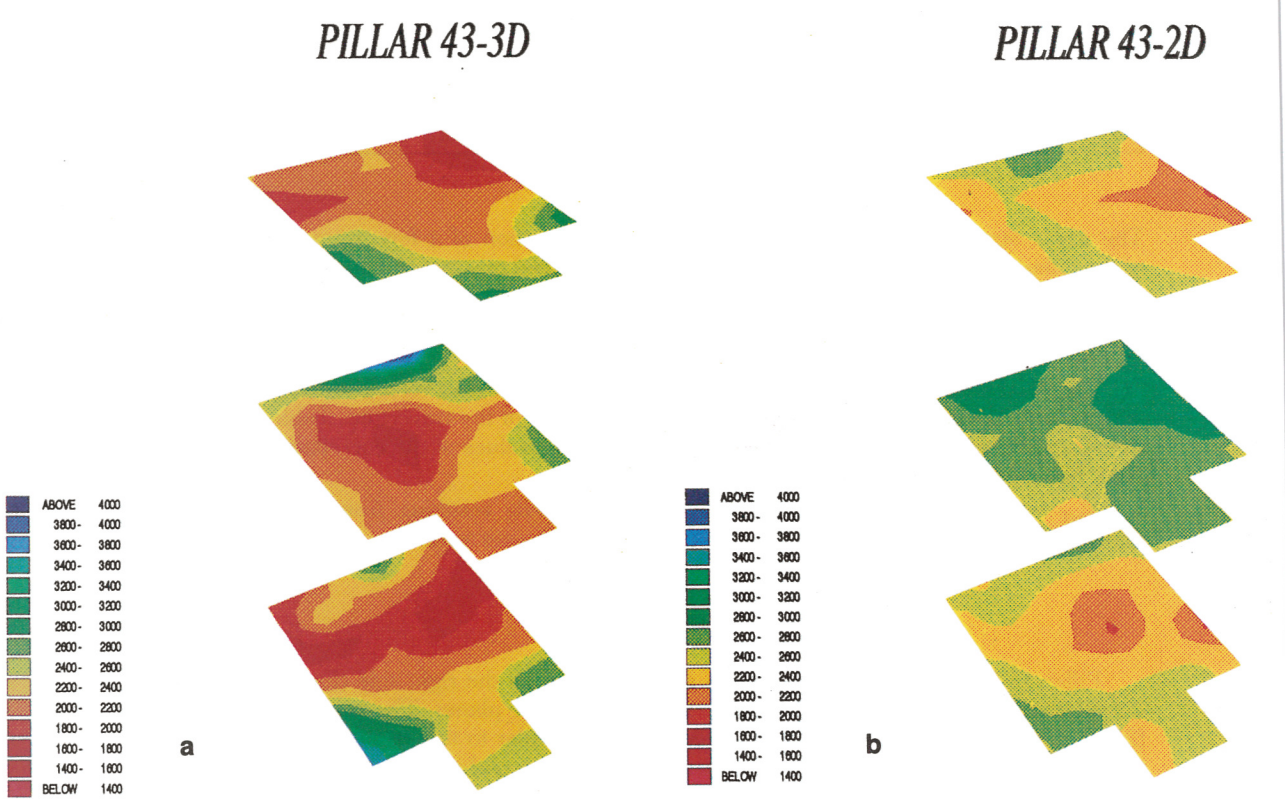


Fig. 3 — 3D (a) and 2D (b) velocity field contours for Pillar 43.

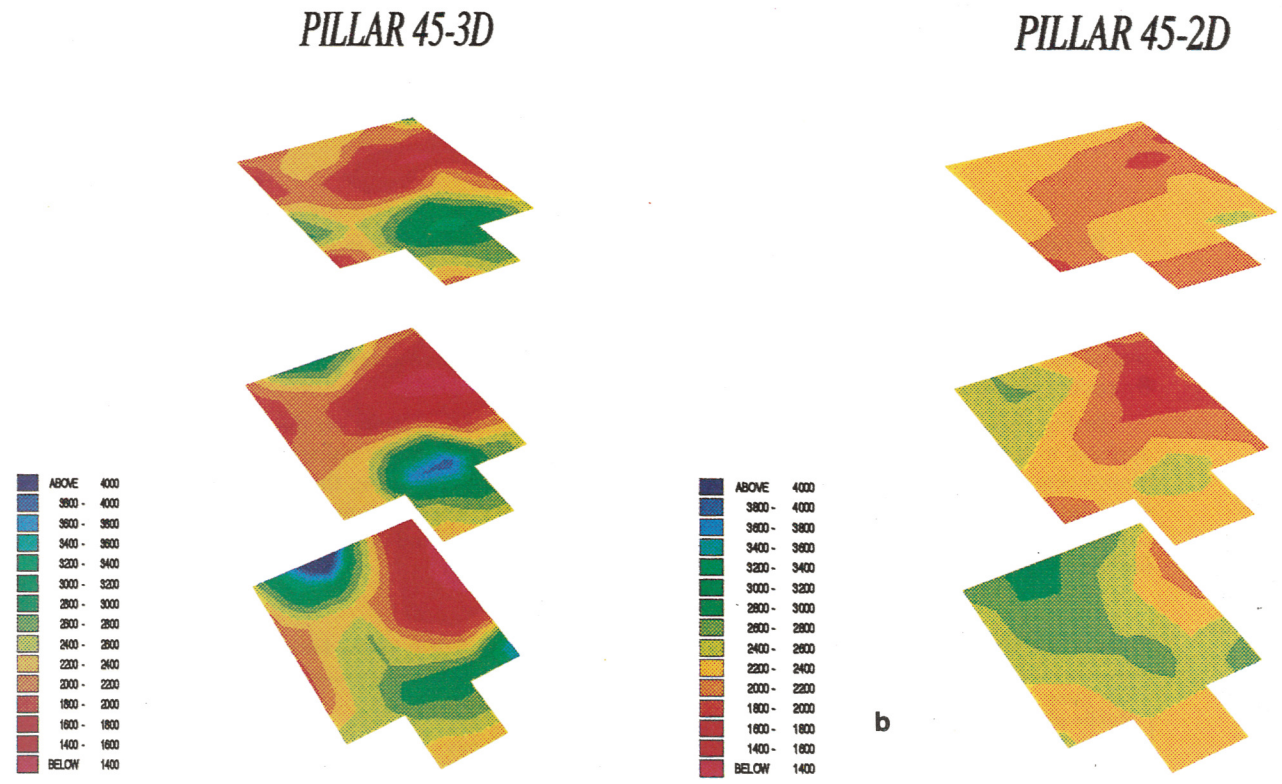


Fig. 4 — 3D (a) and 2D (b) velocity field contours for Pillar 45.

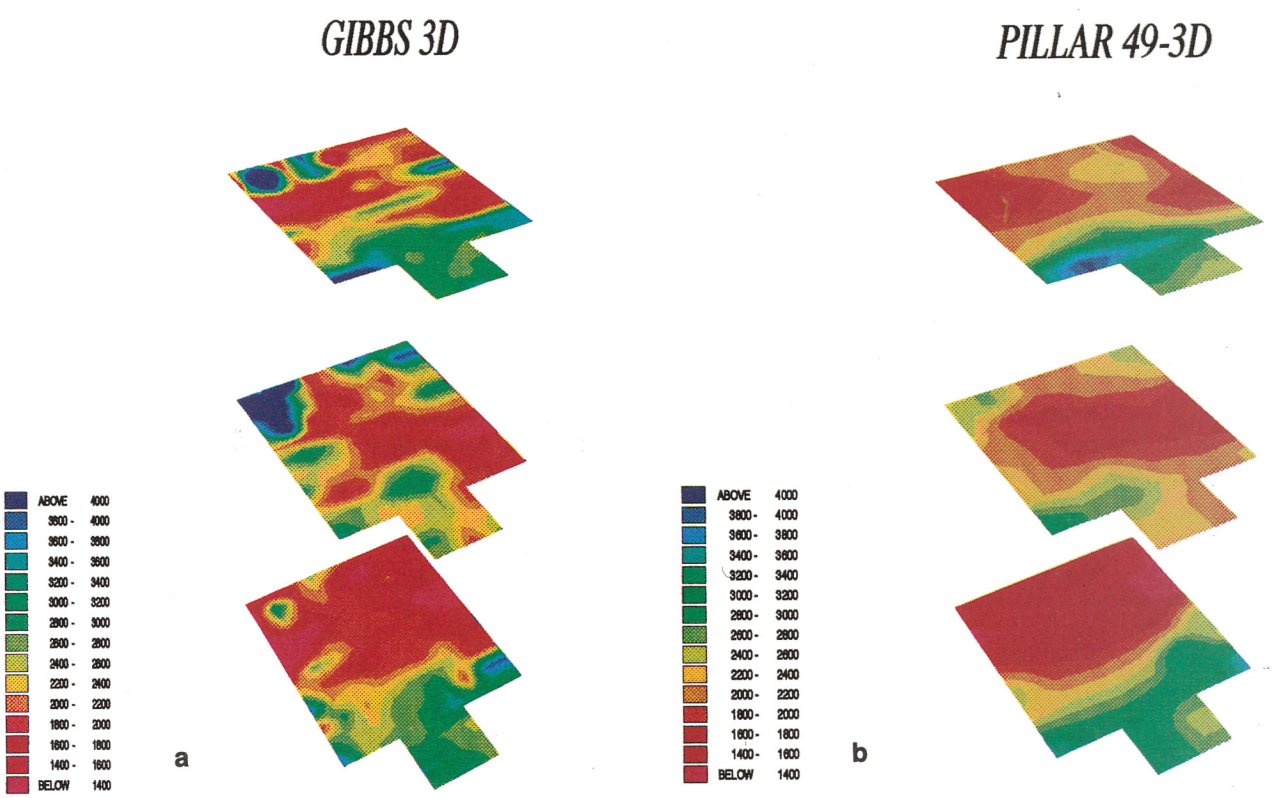


Fig. 5a — 3D (a) and 2D (b) velocity field contours for Pillar 49.

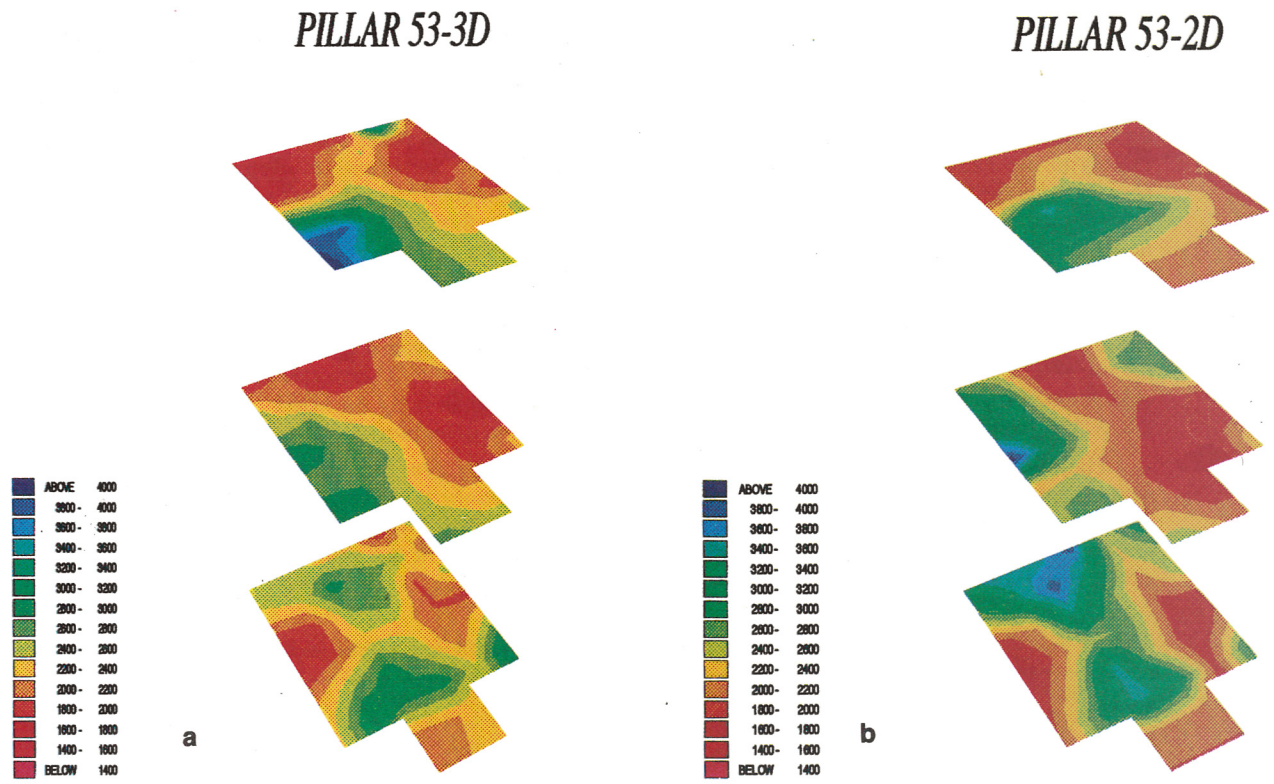


Fig. 6 — 3D (a) and 2D (b) velocity field contours for Pillar 53.

**Table 4 — Pillar 49; 3D and 2D mean velocity and correlation coefficient values for each plane.**

| | | | |
|---|---|---|---|
| Top plane | $V_{mT}$=2350 m/s | $V_{mB}$=2280 m/s | $\sigma$=0.654 |
| Middle plane | $V_{mT}$=2300 m/s | $V_{mB}$=2390 m/s | $\sigma$=0.413 |
| Bottom plane | $V_{mT}$=2200 m/s | $V_{mB}$=1900 m/s | $\sigma$=0.647 |

$V_{mT}$ e $V_{mB}$ are the average velocity values of cells from the 3D and 2D tomography respectively, and $\sigma$ is the correlation coefficent value.

## PILLAR 53

Fig. 6a represents the 3D tomography velocity field of pillar 53. Here, with the exception of two limited low velocity areas (1800-2000 m/s), the pillar appears to be homogeneous, with values of around (2300-2500 m/s). In Fig. 6b, which shows the results of the 2D tomography, the same characteristics as in the 3D tomography are seen. The only exception is in the lower plane where zones of high velocity appear to be more accentuated.

The correlation between the two tomographies appears to be quite good (see Table 5).

$V_{mT}$ e $V_{mB}$ are the average velocity values of cells from the 3D e 2D tomography respectively, and $\sigma$ is the correlation coefficent value.

## CONCLUSIONS

The 3D tomography carried out allowed an evalutation of the average elastic characteristics of the pillars with greater accuracy, and also to determine their variations in space without any increase in acquisition and processing time.

Furthermore comparison with the 2D analysis has allowed us to evaluate some anisotropies which would not otherwise have been identified.

The junction between two blocks did not create an obstacle to the accuracy of first-break times. It should be remembered that travertine is a non-homogeneous material which can show notable differences in its elastic characteristics due to its variable genesis. On this basis, it can be assumed that the variations in velocities recorded for each single pillar are to be attributed mainly to two causes. The first due to the diverse conditions of travertine development, the second because over the centuries each block has been subjected to different effects from environmental pollution and stress generated by the many earthquakes during past centuries in Rome).

The use of tomography contributed in highlighting variations in velocity fields within each pillar. See for example pillar 49, in which variations have been detected on the frontal part of the pillar due to partial substitution of the block, variations which would not have been found by any other type of survey, even seismic. In fact, the histogram in Fig. 2 shows that the average velocities of the seismic rays for each single pillar are approximately the same, at around 2100-2200 m/s. Such homogeneity would not have allowed detection of the variations.

The comparison carried out between the 3D and 2D tomography highlighted some zones with anisotropic fractures. In fact pillar 49, which without doubt has deteriorated the most, presents a velocity field whose average value does not reach 2300 m/s in the 3D tomography nor 2200 m/s in the 2D. This is due to a subvertical orientation of the fractures, especially at the lower end, which can be seen on the surface of the pillar.

**Table 5 — Pillar 53; 3D and 2D mean velocity and correlation coefficient values for each plane.**

| | | | |
|---|---|---|---|
| Top plane | $V_{mT}$=2428 m/s | $V_{mB}$=2237 m/s | $\sigma$=0.663 |
| Middle plane | $V_{mT}$=2284 m/s | $V_{mB}$=2353 m/s | $\sigma$=0.610 |
| Bottom plane | $V_{mT}$=2334 m/s | $V_{mB}$=2530 m/s | $\sigma$=0.652 |

## REFERENCES

Bernabini M., Cancaniccia M. and Cardarelli E.; 1990: *Seismic survey of some pillars of Coliseum (Rome, Italy)*. In: Pernicka E., Wagner G.A. (ed), Archaeometry '90, pp. 677-686.

Nolet G.; 1987: *Seismic wave propagation and seismic tomography*. In: Nolet G. (ed), Seismic Tomography, Reidel, Dordrecht, pp. 1-47.

Paige C.C. and Saunders M.A.; 1982: *LSQR, An algorithm for sparse linear equations and sparse least squares*. In: Rice J.R. (ed), ACM Trans. Math. Softw., New York (U.S.A.), pp. 43-71.

Spakman W. and Nolet G.; 1988: *Imaging algorithms, accuracy and resolution in delay time tomography*. In: Vlaar N.J., Nolet G., Wortel M.J.R. and Cloetingh S.A.P.L. (eds), Mathematical Geophysics, Reidel Dordrecht, pp. 155-187.

Van Der Sluis A. and Van Der Vorst A.; 1987: *Large sparse systems*. In: Nolet G. (ed), Seismic Tomography, Reidel, Dordrecht, pp. 49-83.